Biomedical Optics EXPRESS

A quantitative method for measurement of HL-60 cell apoptosis based on diffraction imaging flow cytometry technique

Xu Yang,[1] Yuanming Feng,[1,2,*] Yahui Liu,[1] Ning Zhang,[1] Wang Lin,[1] Yu Sa,[1,4] and Xin-Hua Hu[3]

[1]*Department of Biomedical Engineering, Tianjin University, Tianjin 300072, China*
[2]*Department of Radiation Oncology, East Carolina University, Greenville, NC 27834, USA*
[3]*Department of Physics, East Carolina University, Greenville, NC 27858, USA*
[4]*sayu@tju.edu.cn*
[*]*fengyu@ecu.edu,*

Abstract: A quantitative method for measurement of apoptosis in HL-60 cells based on polarization diffraction imaging flow cytometry technique is presented in this paper. Through comparative study with existing methods and the analysis of diffraction images by a gray level co-occurrence matrix algorithm (GLCM), we found 4 GLCM parameters of contrast (CON), cluster shade (CLS), correlation (COR) and dissimilarity (DIS) exhibit high sensitivities as the apoptotic rates. It was further demonstrated that the CLS parameter correlates significantly (R^2 = 0.899) with the degree of nuclear fragmentation and other three parameters showed a very good correlations (R^2 ranges from 0.69 to 0.90). These results demonstrated that the new method has the capability for rapid and accurate extraction of morphological features to quantify cellular apoptosis without the need for cell staining.

OCIS codes: (000.1430) Biology and medicine; (170.1530) Cell analysis.

References and links

1. S. Rello, J. C. Stockert, V. Moreno, A. Gámez, M. Pacheco, A. Juarranz, M. Cañete, and A. Villanueva, "Morphological criteria to distinguish cell death induced by apoptotic and necrotic treatments," Apoptosis **10**(1), 201–208 (2005).
2. J. M. Brown and L. D. Attardi, "The role of apoptosis in cancer development and treatment response," Nat. Rev. Cancer **5**(3), 231–237 (2005).
3. J. F. Kerr, A. H. Wyllie, and A. R. Currie, "Apoptosis: a basic biological phenomenon with wide-ranging implications in tissue kinetics," Br. J. Cancer **26**(4), 239–257 (1972).
4. Y. Otsuki, Z. L. Li, and M. A. Shibata, "Apoptotic detection methods--from morphology to gene," Prog. Histochem. Cytochem. **38**(3), 275–339 (2003).
5. E. Ulukaya, C. Acilan, F. Ari, E. Ikitimur, and Y. Yilmaz, "A glance at the methods for detection of apoptosis qualitatively and quantitatively," Turk. J. Bioch **36**, 261–269 (2011).
6. C. S. Chen, M. Mrksich, S. Huang, G. M. Whitesides, and D. E. Ingber, "Geometric Control of Cell Life and Death," Science **276**(5317), 1425–1428 (1997).
7. A. Khmaladze, R. L. Matz, T. Epstein, J. Jasensky, M. M. Banaszak Holl, and Z. Chen, "Cell volume changes during apoptosis monitored in real time using digital holographic microscopy," J. Struct. Biol. **178**(3), 270–278 (2012).
8. Y. A. Lazebnik, S. Cole, C. A. Cooke, W. G. Nelson, and W. C. Earnshaw, "Nuclear events of apoptosis in vitro in cell-free mitotic extracts: a model system for analysis of the active phase of apoptosis," J. Cell Biol. **123**(1), 7–22 (1993).
9. M. M. Martinez, R. D. Reif, and D. Pappas, "Detection of apoptosis: A review of conventional and novel techniques," Anal. Methods **2**(8), 996–1004 (2010).
10. M. van Engeland, L. J. Nieland, F. C. Ramaekers, B. Schutte, and C. P. Reutelingsperger, "Annexin V-affinity assay: a review on an apoptosis detection system based on phosphatidylserine exposure," Cytometry **31**(1), 1–9 (1998).
11. Z. Shiffer, N. Zurgil, Y. Shafran, and M. Deutsch, "Analysis of laser scattering pattern as an early measure of apoptosis," Biochem. Biophys. Res. Commun. **289**(5), 1320–1327 (2001).

#208709 - $15.00 USD Received 25 Mar 2014; revised 13 May 2014; accepted 8 Jun 2014; published 11 Jun 2014

12. G. C. Salzman, J. M. Crowell, C. A. Goad, K. M. Hansen, R. D. Hiebert, P. M. LaBauve, J. C. Martin, M. L. Ingram, and P. F. Mullaney, "A flow-system multiangle light-scattering instrument for cell characterization," Clin. Chem. **21**(9), 1297–1304 (1975).
13. A. N. Shvalov, I. V. Surovtsev, A. V. Chernyshev, J. T. Soini, and V. P. Maltsev, "Particle classification from light scattering with the scanning flow cytometer," Cytometry **37**(3), 215–220 (1999).
14. K. M. Jacobs, L. V. Yang, J. Ding, A. E. Ekpenyong, R. Castellone, J. Q. Lu, and X. H. Hu, "Diffraction imaging of spheres and melanoma cells with a microscope objective," J. Biophotonics **2**(8-9), 521–527 (2009).
15. J. Neukammer, C. Gohlke, A. Höpe, T. Wessel, and H. Rinneberg, "Angular distribution of light scattered by single biological cells and oriented particle agglomerates," Appl. Opt. **42**(31), 6388–6397 (2003).
16. X. T. Su, K. Singh, C. Capjack, J. Petrácek, C. Backhouse, and W. Rozmus, "Measurements of light scattering in an integrated microfluidic waveguide cytometer," J. Biomed. Opt. **13**(2), 024024 (2008).
17. K. M. Jacobs, J. Q. Lu, and X. H. Hu, "Development of a diffraction imaging flow cytometer," Opt. Lett. **34**(19), 2985–2987 (2009).
18. Z. Darzynkiewicz, S. Bruno, G. Del Bino, W. Gorczyca, M. A. Hotz, P. Lassota, and F. Traganos, "Features of apoptotic cells measured by flow cytometry," Cytometry **13**(8), 795–808 (1992).
19. M. G. Ormerod, F. Paul, M. Cheetham, and X. M. Sun, "Discrimination of apoptotic thymocytes by forward light scatter," Cytometry **21**(3), 300–304 (1995).
20. J. R. Mourant, J. P. Freyer, A. H. Hielscher, A. A. Eick, D. Shen, and T. M. Johnson, "Mechanisms of light scattering from biological cells relevant to noninvasive optical-tissue diagnostics," Appl. Opt. **37**(16), 3586–3593 (1998).
21. J. Q. Lu, P. Yang, and X. H. Hu, "Simulations of Light scattering from a biconcave red blood cell using the finite-difference time-domain method," J. Biomed. Opt. **10**, 024022 (2005).
22. H. Ding, J. Q. Lu, R. S. Brock, T. J. McConnell, J. F. Ojeda, K. M. Jacobs, and X. H. Hu, "Angle-resolved Mueller matrix study of light scattering by B-cells at three wavelengths of 442, 633, and 850 nm," J. Biomed. Opt. **12**(3), 034032 (2007).
23. K. Dong, Y. Feng, K. M. Jacobs, J. Q. Lu, R. S. Brock, L. V. Yang, F. E. Bertrand, M. A. Farwell, and X. H. Hu, "Label-free classification of cultured cells through diffraction imaging," Biomed. Opt. Express **2**(6), 1717–1726 (2011).
24. S. Yu, J. Zhang, M. S. Moran, J. Q. Lu, Y. Feng, and X. H. Hu, "A novel method of diffraction imaging flow cytometry for sizing microspheres," Opt. Express **20**(20), 22245–22251 (2012).
25. J. Zhang, Y. Feng, M. S. Moran, J. Q. Lu, L. V. Yang, Y. Sa, N. Zhang, L. Dong, and X. H. Hu, "Analysis of cellular objects through diffraction images acquired by flow cytometry," Opt. Express **21**(21), 24819–24828 (2013).
26. B. A. Wagner, G. R. Buettner, L. W. Oberley, C. J. Darby, and C. P. Burns, "Myeloperoxidase is involved in H_2O_2-induced apoptosis of HL-60 human leukemia Cells," J. Biol. Chem. **275**(29), 22461–22469 (2000).
27. D. Peus, R. A. Vasa, A. Meves, M. Pott, A. Beyerle, K. Squillace, and M. R. Pittelkow, "H_2O_2 is an important mediator of UVB-induced EGF-receptor phosphorylation in cultured keratinocytes," J. Invest. Dermatol. **110**(6), 966–971 (1998).
28. A. Mauguen, J. P. Pignon, S. Burdett, C. Domerg, D. Fisher, R. Paulus, S. J. Mandrekar, C. P. Belani, F. A. Shepherd, T. Eisen, H. Pang, L. Collette, W. T. Sause, S. E. Dahlberg, J. Crawford, M. O'Brien, S. E. Schild, M. Parmar, J. F. Tierney, C. Le Pechoux, and S. Michiels; Surrogate Lung Project Collaborative Group, "Surrogate endpoints for overall survival in chemotherapy and radiotherapy trials in operable and locally advanced lung cancer: a re-analysis of meta-analyses of individual patients' data," Lancet Oncol. **14**(7), 619–626 (2013).
29. G. Koopman, C. P. Reutelingsperger, G. A. Kuijten, R. M. J. Keehnen, S. T. Pals, and M. H. J. van Oers, "Annexin V for flow cytometric detection of phosphatidylserine expression on B cells undergoing apoptosis," Blood **84**(5), 1415–1420 (1994).
30. Y. Sa, Y. Feng, K. M. Jacobs, J. Yang, R. Pan, I. Gkigkitzis, J. Q. Lu, and X. H. Hu, "Study of low speed flow cytometry for diffraction imaging with different chamber and nozzle designs," Cytometry A **83**(11), 1027–1033 (2013).
31. R. M. Haralick, "Statistical and structural approaches to texture," Proc. IEEE **67**(5), 786–804 (1979).
32. S. V. Buggenhout, T. Grauwet, A. V. Loey, and M. Hendrickx, "Structure/processing relation of vacuum infused strawberry tissue frozen under different conditions," Eur. Food Res. Technol. **226**(3), 437–448 (2008).
33. X. F. Yang, S. Tridandapani, J. J. Beitler, D. S. Yu, E. J. Yoshida, W. J. Curran, and T. Liu, "Ultrasound GLCM texture analysis of radiation-induced parotid-gland injuryin head-and-neck cancer radiotherapy: An in vivo study of late toxicity," Med. Phys. **39**, 5732–5739 (2012).
34. R. W. Conners, M. M. Trivedi, and C. A. Harlow, "Segmentation of a high-resolution urban scene using texture operators," Comput. Vis. Graph. Image Process. **25**(3), 273–310 (1984).

1. Introduction

As a process of programmed cell death, apoptosis plays a fundamental role in maintenance of the physiological balance and response to pathological conditions [1]. In addition to its importance in basic cell biology and biophysical research, the apoptosis related mechanisms are at the root of multiple human diseases including cancers, autoimmunity and degenerative disorders and study of apoptosis attracts active research interests [2]. In the case of cancer

#208709 - $15.00 USD Received 25 Mar 2014; revised 13 May 2014; accepted 8 Jun 2014; published 11 Jun 2014

treatment, for example, apoptosis affects profoundly a patient's response to therapy and recurrence risk due to the close relationship between the sensibility of tumor cells to the treatment regime and the microenvironment. Therefore, quantitative measurement of cell apoptosis to assess patients' responses becomes increasingly important for individualized therapy [2,3].

It has been widely accepted that cell apoptosis starts in response to molecular stimulations and undergoes a sequence of signal pathways that leads to characteristic morphological changes [3]. A number of methods have been developed for apoptosis detection. Since cell dehydration occurs in the early stage of apoptosis, loss of intracellular water causes cellular shrinking, condensation of the cytoplasm and marginalization of the chromatin which results in change in cell size. Therefore, nuclear fragmentation serves as a morphological hallmark of cellular apoptosis. In the late stage of apoptosis, membrane ruffles and blebs and eventually breaks up to form the apoptotic bodies [1,4]. Microscopic means have been used to study the morphological features of apoptotic cells stained with fluorescent dyes [4,5]. Imaging of unstained apoptotic cells have also been performed with phase contrast microscopy and digital holography [6,7]. Microscopic imaging analysis yields explicit information on the change of cellular structure in different stages of apoptosis. But these methods are very labor intensive and provide often qualitative results because of the difficulty to quantify cellular morphology.

Due to the difficulty for morphological measurements, apoptosis detection is mostly carried out presently through molecular analysis. An extensively used method is to determine the degree of cleavage of nuclear DNA that can be visualized as a characteristic nucleosomal ladder in agarose gel by electrophoresis [5,8]. Other molecular assays are available which include the TUNEL assay utilizing the TDT and fluorescein to determine the DNA breakpoints in apoptosis and the ELISA assay to detect internucleosomal DNA fragments. Unfortunately, it is difficult to apply these assays to quantify and evaluate apoptosis conditions in single cells. For rapid assay of single cells, a method of flow cytometry (FCM) has become attractive to many investigators for its capability to measure light scatter and fluorescence signals simultaneously at high speed [9]. A standard FCM assay consists of cell staining with two fluorescent reagents, Annexin V-FITC and propidium iodide (PI) followed by flow measurement [10]. Annexin V binds to phosphatidylserine (PS) translocated from the inner to the outer leaflets of the cytoplasmic membrane in early stage which can be separated from PI permeated cells with compromised membranes in late stage. Therefore, an FCM assay with the two reagents enables discrimination of apoptotic cells in early and late stages.

While the molecular assays including the FCM assay can present characteristic molecular signals associated with the apoptosis, they usually yield no or very limited information on cell morphology and thus are of indirect nature in apoptosis detection. Furthermore, molecular assays typically require cell staining with multiple fluorescent reagents which increase the complexity in sample preparation, measurement and data analysis, often significantly, and the cost of study as well. Consequently, it is highly desired to develop rapid and accurate methods for quantitative measurement of apoptosis in single cells that allows detailed analysis of cell morphology. Previous studies have been reported to extract morphological information from angle-resolved measurement of coherent light scatters recorded by linear array sensors [11,12], time-of-flight detection for angle-resolved measurement [13] or image sensors [14–17]. In particular, angle-resolved measurement of coherent forward light scatters has been performed on apoptotic cells excited by a laser beam with a linear array detector to determine the cell sizes [11]. In fact, it can be readily observed that apoptotic cells distribute differentially from the viable cells in a scatter plot of the angularly integrated side scatters (SSC) versus the forward scatters (FSC) obtained with the FCM assay [18,19]. These results suggest some strong correlations between the morphological variations in apoptotic cells relative to the viable cells and spatial distribution of scattered light, which are consistent with the experimental and modeling studies on light scattering by biological cells of different morphology in general [15–17,20–25].

#208709 - $15.00 USD Received 25 Mar 2014; revised 13 May 2014; accepted 8 Jun 2014; published 11 Jun 2014

Despite the well-known strong correlation as discussed above, no rapid and label-free protocols are available to quantify and measure cellular apoptosis. We have recently developed a polarization diffraction imaging flow cytometry (p-DIFC) method and shown its capacity for cell characterization and classification without fluorescent staining [17,23–25]. Different from the FCM assay, the p-DIFC measurement records the spatial distribution of coherent light scatters from single cells excited by a laser beam with cameras and extracts the diffraction pattern or texture features from the acquired images. In this report, we present our first experimental study of apoptosis in HL-60 cells induced by the H_2O_2 treatment with the p-DIFC method. The cross-polarized diffraction image pairs acquired from the cells were analyzed with a gray level co-occurrence matrix (GLCM) algorithm to obtain parameters of image texture and pixel intensity for quantitative cell characterization. By examining the dependence of the extracted image parameters on the post-treatment time, we have identified 4 GLCM parameters that are sensitive to the treatment of the cells with reduced fluctuations between different samples. Fluorescence microscopy and FCM assay of the treated cells have been conducted to provide baseline data on the morphological variations and apoptotic rates for evaluation and validation of the p-DIFC method as a new tool for measurement of apoptosis in single cells.

2. Materials and methods

2.1 Cell culture and H_2O_2 treatment

The HL-60 human promyelocytic leukemia cell line [26] was used in this study with cells grown at 37°C in a 5% CO_2 and 95% air atmosphere in suspension in the RPMI 1640 media (Gibco) supplemented with 10% fetal calf serum (FCS, Gibco), 100U/ml penicillin and 100U/ml streptomycin. The cell samples were sub-cultured every third day when the cell density reached the value of 5×10^6 cells/ml. Annexin V-FITC/PI assay kit (BD Biosciences) and Hoechst 33342 (Invitrogen) were used to stains the cells for FCM measurement and microscopic observation.

To induce the HL-60 cells into apoptosis, we employed the well-studied method of treating cells with the reactive oxygen species of hydrogen peroxide (H_2O_2) [26,27]. The HL-60 cells in the log phase were pelleted and re-suspended in the RPMI-1640 without FCS to synchronize by serum deprivation for 6 hours. After the synchronization, FCS was added to obtain the complete medium for cell treatment. Five aliquot samples were prepared from each cell suspension with the density set to about 5×10^5 cells/ml and each sample was further divided into two equal portions with one as control and the other treated by H_2O_2. Apoptosis in HL-60 cells were induced by incubating the cells in the culture media with H_2O_2 (Sigma-Aldrich) added at the 1.5mM concentration for 0h, 3h, 6h, 12h and 24h, respectively, before measurement.

2.2 Experimental design

Treated cell samples were pelleted by centrifugation at 200 × g for 3min and washed once with phosphate-buffered saline (PBS, PH 7.2-7.6, Gibco) before measurement. The time of cell incubation in the medium with H_2O_2 before the wash is defined as the post-treatment time t_p. The H_2O_2 induced apoptosis in treated cell samples was quantified at each t_p by three methods: 1) microscopic analysis of morphological change, 2) Annexin V-FITC/PI assay with the FCM assay, and 3) acquisition and analysis of cross-polarized diffraction images with the p-DIFC method. The fluorescence microscopy and FCM assay were designed to provide baseline data against which the p-DIFC method was to be evaluated and validated. All cell measurements with each of the three methods were repeated for three times to obtain mean values and standard deviations (SD) of the data such as the apoptosis rate and morphological parameters. The coefficient of determination (R^2) was calculated for analysis of correlations between the t_p dependence of the results obtained with different methods. Correlations are characterized as excellent for $R^2 \geq 0.90$, very good for $0.90 < R^2 \leq 0.75$,

#208709 - $15.00 USD Received 25 Mar 2014; revised 13 May 2014; accepted 8 Jun 2014; published 11 Jun 2014

good for $0.75 < R^2 \leq 0.50$, moderate for $0.50 < R^2 \leq 0.25$ and poor for $R^2 < 0.25$ [28]. Statistical analysis was performed with SigmaPlot (12.0, Systat Software).

2.3 Cell preparation

Control and treated cell samples were triply stained for morphological measurement through microscopy and doubly stained for FCM assay for detection of apoptosis. Hoechst 33342, Annexin V-FITC and PI were used to stain the cells for morphological characterization by an inverted fluorescence microscope equipped with an Xcellence imaging workstation (IX71, Olympus). As a DNA banding agent, the Hoechst 33342 dye was employed to allow detailed analysis of the nuclear morphology for both viable and apoptotic cells. In our study, Hoechst 33342 and Annexin V binding buffer were diluted respectively to 1/30 and 1/10 of original concentration with PBS. The cell pellet was re-suspended in the buffer with the cell density adjusted to 3 to 6×10^5 cells/ml, and 100μl of the suspension was incubated with 5μl Hoechst 33342 and 5μl Annexin V-FITC for 10min in dark at room temperature and subsequently incubated with 5μl PI for another 5min.

2.4 Microscopy and FCM assays

The stained cells were washed once and re-suspended to a concentration of about 1×10^6 cells/ml in the buffer. A small portion of 15 to 20μl was placed on a glass slide with a top cover glass for microscopy with fluorescence light of the three reagents collected respectively into three color channels of an image file. Early apoptotic cells can be separated from the late apoptotic cells according to whether they can be stained by Annexin V-FITC only or together with PI [10,29]. To analyze quantitatively the morphological changes in single cells, we utilized the image processing software provided by Olympus to calculate 14 characteristic parameters from each cell. Additionally, we determined the apoptotic rate P_a defined as the number ratio of the positive Annexin V-FITC cells to the analyzed cells for each sample. The value of P_a measured from the control cell sample was subtracted from that of the treated cell sample to compensate the effect of apoptosis induced by causes other than H_2O_2. Furthermore, we characterized the changes in nuclear morphology for each treated cell sample by a percentage of cells with fragmented nuclei to the analyzed cells. The PFN was determined visually by the existence of gaps characteristic of nuclear fragmentation in cells stained by Hoechst 33342. The dependence of PFN on t_p of treated cell samples was obtained for comparison with the variations in the texture parameters of the diffraction images acquired by the p-DIFC method.

The FCM assay was applied to quantify apoptosis in H_2O_2 treated cells samples at different t_p under the standard Annexin V-FITC/PI assay protocol [10,29]. Treated cell samples were centrifuged and re-suspended with 500μl buffer for measurement with a conventional flow cytometer (Calibur, BD Biosciences) using the excitation wavelengths of 488nm for Annexin V-FITC (FL1) and PI (FL2). For each measurement, a sample of unstained viable cells was measured first to obtain forward scatter (FSC) and side scatter (SSC) signals for gating of the measured signals from the treated sample to reduce the influence of cell debris. The apoptotic rate P_a was determined according to the definition described above.

2.5 p-DIFC measurement and image analysis

Heterogeneous distribution of refractive index inside cells causes elastic light scattering in the form of light scatters in space. To determine their spatial distribution, we acquired and analyzed the diffraction images from treated cells using a p-DIFC prototype system (WavMed Technologies). Control and treated cell samples of 1ml in volume and 1×10^5 cells/ml in concentration were prepared in the RPMI 1640 media. The cell suspension in a sample was drawn into the system as the core fluid to form a laminar flow in the flow chamber with a sheath fluid. The flow chamber was made of quartz glass with a square channel of 3mm side and 40mm length. A stainless tube of 130μm inside diameter fixed

#208709 - $15.00 USD Received 25 Mar 2014; revised 13 May 2014; accepted 8 Jun 2014; published 11 Jun 2014

along the center of the square channel separates the core fluid from the sheath at the top portion of the flow chamber. Results of detailed simulation and experimental measurement of the speed distribution and laminar flow have been published previously [30].

After injection, cells moved in single file through the focus of an incident laser beam of 532nm in wavelength and about 40mW in power [17,25]. The coherent light scatters along the side directions were collected by an infinity-corrected objective of 50x (378-805-3, Mitutoyo) and divided into two cross-polarized (s-polarized and p-polarized) components by a polarizing beam splitter. The spatial distributions of the polarized scattered light intensity were recorded by two 12-bit CCD cameras (LM075M, Lumenera) as a pair of cross-polarized diffraction images. The imaging unit consisting of the objective, beam splitter, tube lenses and cameras was first focused on the core fluid and the focal spot of the incident beam. At this location the imaging unit has a resolution of about 0.6μm and collects the scattered light over an angular range of about $\Delta\theta_s = \pm 18°$ in polar angle and $\Delta\varphi_s = \pm 14°$ in azimuthal angle with respect to the direction of incident beam defining the z-axis. To acquire diffraction images, the imaging unit was translated as whole to an off-focus position of 100μm towards the flow chamber. The off-focus imaging is necessary to obtain diffraction images that highly correlated to the morphology of the coherently illuminated cellular object as discussed in [14]. An exposure time of 0.5ms was set for the two cameras in diffraction image acquisition with the flow speed of the cells adjusted to about 5mm/s.

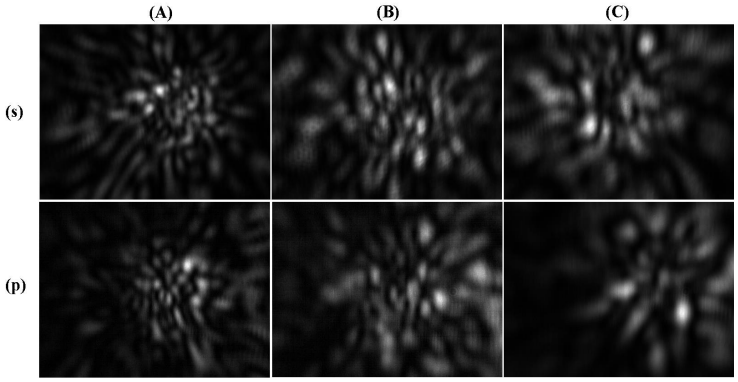

Fig. 1. Examples of diffraction image pairs acquired from individual flowing cells with light wavelength of $\lambda = 532$nm, exposure time of $t = 0.5$ms and different post-treatment time t_p; (A) $t_p = 0$h; (B) $t_p = 6$h; (C) $t_p = 24$h. The letters of s and p stand for s-polarization and p-polarization of the scattered light respectively.

About 1000 pairs of raw images were acquired from each measured cell sample at different t_p. We have developed image processing software to automate the image analysis consisting of pre-screening and calculation of image parameters. The acquired 12-bit image files were processed to eliminate the images of over-exposure and under-exposure before normalized into 8-bit image files. The software then removed the image pairs with large speckles which have been shown to be formed by the coherent scatters from cellular debris or cells with significantly damaged and reduced structures [23]. Figure 1 presents examples of diffraction image pairs obtained after pre-screening. The pre-screening part of the software usually removed about 20% to 30% of the raw image pairs. The remaining pairs of cross-polarized diffraction images were then processed with a GLCM algorithm for quantitative characterization of the fringe patterns presented by a diffraction image as the image texture and pixel intensity parameters. Details of the GLCM calculation have been presented previously [23]. Briefly, the GLCM algorithm characterizes image textures by constructing a matrix whose elements are defined as the occurrence probability of paired intensities or gray levels at two neighboring pixels in the input image [31]. For our study, we extracted a total of 38 image texture and pixel intensity parameters from each diffraction image pair per cell to

#208709 - $15.00 USD Received 25 Mar 2014; revised 13 May 2014; accepted 8 Jun 2014; published 11 Jun 2014

investigate their dependence on post-treatment time t_p and correlations with the data acquired through microscopy and FCM assays.

3. Results

3.1 Morphological analysis through fluorescence microscopy

Triply stained control and H_2O_2 treated cells samples were analyzed with the fluorescence microscopy by acquiring four to six images of 1367 × 1038 pixels with a field-of-view of 440μm × 335μm from each sample. Typical images of the stained cells are shown in Fig. 2. The characteristic changes in apoptotic cells such as cell shrinking, chromatin clumping and nuclear fragmentation can be clearly observed in these images, which confirmed that the HL-60 cells in the treated sample were driven into the apoptosis process. To determine the apoptotic rate P_a of each cell sample, we selected randomly about 200 cells from the acquired images and separated them into three groups according to the emitted fluorescence: the viable group with positive Hoechst 33342 and negative FITC and PI, the early apoptosis group with positive FITC and negative PI and late apoptosis group with positive FITC and PI. The same rate was also determined from the control sample and subtracted from those of the treated samples to compensate for apoptosis by causes other than H_2O_2. Different from P_a, PFN was determined solely on the ground of nuclear integrity by Hoechst 33342.

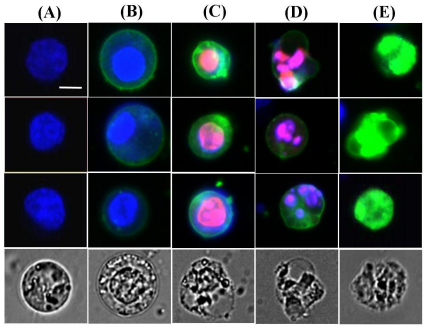

Fig. 2. Microscopic images of the HL-60 cells with morphological changes at different apoptotic stages induced by H_2O_2. Hoechst 33324 fluorescence shows in blue, Annexin V-FITC fluorescence shows in green and PI fluorescence shows in red: (A) viable cells; (B) early apoptotic cells; (C) late apoptotic and necrotic cells; (D) cells with nuclear fragments; (E) enucleated cells and apoptotic bodies. The bottom row shows bright-field images. Bar = 10μm.

To quantify the morphological change, we calculated 14 morphological parameters for each analyzed cell by manually sketching the cellular and nuclear membranes of the selected cell using the Xcellence imaging workstation. The standard parameters for characterization of 2D morphology have been calculated that include the area, perimeter, equivalent circle diameter (ECD), sphericity, elongation and aspect ratio [32] for the cell and its nucleus, etc. The results of the 14 parameters are listed in Table 1. Among these, the nucleus-to-cell ratio (NCR) measures directly the change in nuclear volume relative to the cell. We further defined three parameters to characterize the shape variation. The parameter of diameter mean is calculated as the arithmetic mean value of cellular diameters measured from 0° through 179° in rotation angle with a step of 1°. The parameters of diameter max and diameter inner max (DIM) quantify the degree of nuclear shrinkage with the former defined as maximum nuclear diameter and the latter as the maximum nuclear diameter with no portion external to the nucleus. To investigate the statistical significance of the parameter variations among the three cell groups, we pool the values of the 2D morphological parameter calculated from the selected cells of all samples.

We have also determined P_a and PFN through microscopic analysis of treated cell samples against t_p. The dependence of P_a and PFN on t_p are plotted in Fig. 3(C) together with P_a determined by the FCM assay for comparison. Excellent agreement with $R^2 = 0.975$ can

#208709 - $15.00 USD Received 25 Mar 2014; revised 13 May 2014; accepted 8 Jun 2014; published 11 Jun 2014

be seen between the two rate data sets of morphological analysis and FCM assay which clearly shows the repeatability of the H_2O_2 treatment to induce apoptosis in the HL-60 cells for this study. Quantitative analysis of the correlation between PFN and P_a by FCM shows strong correlation between the two data sets with $R^2 = 0.895$. These results indicate strongly that PFN provides a morphological metric for quantitative measurement of apoptosis equivalent to the apoptotic rate P_a determined by molecular probes. Still, the microscopic determination of PFN and other morphological parameters are extremely labor intensive and time consuming.

Table 1. Morphological parameters measured with the fluorescence microscopy method*

Parameters[!]		Cell conditions			One-way ANOVA test		
		VC[#]	EAC[#]	LAC[#]	VC-EAC	VC-LAC	EAC-LAC
Cell	A (μm^2)	169 ± 3.0	153 ± 1.1	149 ± 2.4	$p = 0.002$	$p = 0.002$	$p = 0.109$
	P (μm)	49.7 ± 0.40	45.6 ± 2.8	45.2 ± 0.17	$p = 0.040$	$p = 0.042$	$p = 0.789$
	ECD (μm)	16.6 ± 0.95	13.9 ± 0.88	13.6 ± 0.099	$p = 0.009$	$p = 0.009$	$p = 0.648$
	Sphericity	0.854 ± 0.011	0.770 ± 0.020	0.746 ± 0.011	$p<0.001$	$p<0.001$	$p = 0.091$
	Shape factor	0.930 ± 0.020	0.890 ± 0.0075	0.882 ± 0.0046	$p = 0.016$	$p = 0.010$	$p = 0.459$
	Elongation	1.02 ± 0.069	1.16 ± 0.017	1.17 ± 0.011	$p = 0.022$	$p = 0.020$	$p = 0.669$
	Aspect Ratio	1.10 ± 0.014	1.16 ± 0.016	1.18 ± 0.010	$p = 0.003$	$p = 0.001$	$p = 0.217$
Nucleus	A (μm^2)	79.9 ± 3.4	56.53 ± 2.5	50.64 ± 2.2	$p<0.001$	$p<0.001$	$p = 0.027$
	P (μm)	37.4 ± 1.2	33.3 ± 1.7	31.6 ± 1.1	$p = 0.017$	$p = 0.005$	$p = 0.166$
	ECD(μm)	11.4 ± 1.2	8.18 ± 0.23	7.84 ± 0.079	$p = 0.002$	$p = 0.002$	$p = 0.569$
	D_{av} (μm)	12.3 ± 1.3	9.34 ± 0.32	8.87 ± 0.15	$p = 0.006$	$p = 0.004$	$p = 0.480$
	D_{max} (μm)	13.3 ± 1.4	10.3 ± 0.41	9.64 ± 0.17	$p = 0.008$	$p = 0.005$	$p = 0.411$
	DIM(μm)	11.8 ± 0.29	9.89 ± 0.33	9.47 ± 0.081	$p<0.001$	$p<0.001$	$p = 0.098$
NCR		0.470 ± 0.025	0.370 ± 0.14	0.326 ± 0.011	$p<0.001$	$p<0.001$	$p = 0.023$

* The mean and standard deviation values were obtained from three measurements of the control and treated cells at different t_p, the total numbers of the analyzed cells in three measurements are 716, 722, 709 for the viable cell group, 215, 219, 211 for the early apoptosis cell group and 265, 250, 281 for late apoptosis cell group which may also contain necrotic cells.

[!] A = area; P = perimeter; ECD = equivalent circle diameter; D_{av} = mean value of diameter; D_{max} = maximum diameter; DIM = diameter inner max; NCR = nucleus-to-cell ratio.

[#] VC = viable cell group; EAC = early apoptosis cell group; LAC = late apoptosis cell group.

3.2 FCM assay

The Annexin V-FITC/PI assay of the control and H_2O_2 treated cell samples has been performed with FCM to determine the apoptotic rate P_a by the fluorescence signals as shown in Fig. 3(A) and 3(B). The scatter plot of the control samples of viable cells in Fig. 3(A) was used to divide the plane so that nearly all of the dots representing the measured cells cluster in the LL quadrant. The placing of lines to obtain the four quadrants and calculate the apoptotic rate P_a, however, was empirical by an experienced researcher familiar with the FCM assay. Figure 3(C) shows the dependence of P_a on t_p of different cell samples together with that determined through fluorescence microscopy. Despite the fact that the FCM assay serves as a rapid method to measure apoptosis, it can be observed that uncertainty does exist

#208709 - $15.00 USD Received 25 Mar 2014; revised 13 May 2014; accepted 8 Jun 2014; published 11 Jun 2014

in determining P_a through FCM since the lines dividing the four quadrants in Fig. 3(A) and 3(B) are chosen subjectively instead of objectively according to the assay protocol.

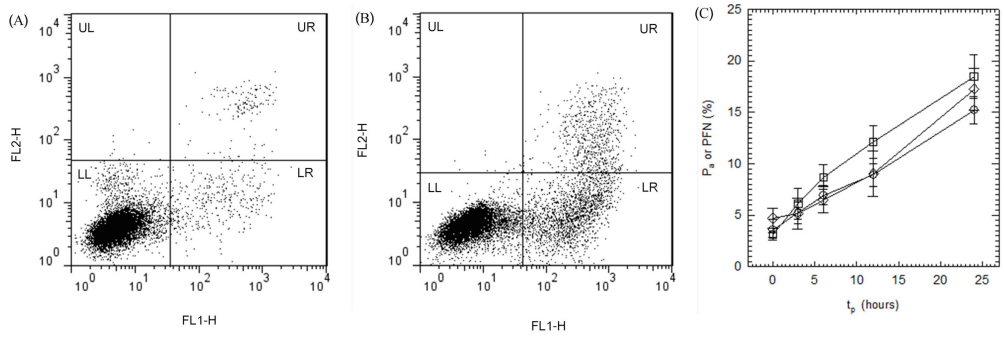

Fig. 3. Typical scatter plots of FL1 vs FL2 signals from 10,000 HL-60 cells of (A) control and (B) H_2O_2 treatment with t_p = 24 (hours) acquired by the Annexin V-FITC/PI assay of FCM. The cell numbers in the four quadrants of LL, LR, UL and UR were used to obtain the apoptotic rate P_a. P_a and PFN are plotted against the post-treatment time t_p in (C) with the diamond, circle and square symbols representing respectively the mean values of P_a with the FCM assay, the microscopy assay and PFN. The error bars represent the standard deviations obtained from three measurements. The lines connecting the symbols are auxiliary for view.

3.3 p-DIFC measurement and image analysis

Control and H_2O_2 treated samples of HL-60 cells were measured by the p-DIFC prototype system to obtain cross-polarized diffraction image pairs from single cells in each sample. The acquired image data after pre-screening were processed by the GLCM based software to obtain 38 texture and pixel intensity parameters for each cross-polarized diffraction image pair per imaged cell. The 38 parameters consist of 19 pairs of identical parameters from each diffraction image in a pair and are labeled by the prefix of s- or p- before the parameter name to denote the polarization of the coherently scattered light recorded by each image. The mean values and standard deviations of these parameters from the measured samples were obtained to examine their dependence on t_p. We have identified 4 GLCM texture parameters that are sensitive to t_p with reasonably small fluctuations between samples as shown in Fig. 4.

The 4 GLCM parameters depicted in Fig. 4 shows different dependence. The parameter of s-CLS and p-COR increase with t_p while p-CON and p-DIS decreases. An examination of the GLCM parameter definitions [23,31] reveals that CLS measures the skewness of a texture pattern for gauging the perceptual concepts of uniformity while COR characterizes the degree of correlation in the paired pixels on their gray levels [30]. On the other hand, CON quantifies the local pattern variations presented in an image, which correlates highly with the difference between the lowest and highest values of pixel intensities within a region of interest [33]. DIS is another feature parameter to describe the contrast of the image besides the CON parameter. The results of microscopy and FCM assays prove that cell samples of increasing t_p contain higher percentages of apoptotic cells, as show in Fig. 3(C). Therefore, the results presented in Fig. 4 provide strong evidences that the p-DIFC method has the capability to characterize cells undergoing apoptosis and measure apoptosis in single cells.

#208709 - $15.00 USD Received 25 Mar 2014; revised 13 May 2014; accepted 8 Jun 2014; published 11 Jun 2014

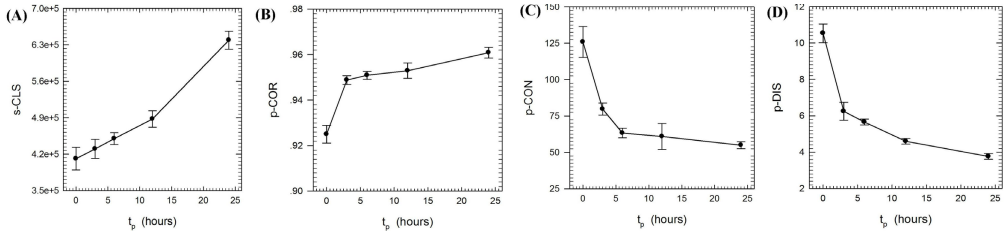

Fig. 4. Four GLCM parameters extracted from the diffraction images of HL-60 cells after being treated with 1.5mM H_2O_2 for 0h, 3h, 6h, 12h and 24h after synchronization through serum deprivation for 6 hours. (A) s-cluster shade (s-CLS); (B) p-correlation (p-COR); (C) p-contrast (p-CON); (D) p-dissimilarity (p-DIS). The lines connecting the symbols are auxiliary for view.

To further evaluate the p-DIFC results against the morphology of the apoptotic cells and the apoptotic rates, we calculated the values of R^2 on the t_p dependence between the 4 GLCM parameters and PFN determined by microscopy and between the GLCM parameters and P_a by FCM. The results are summarized in Table 2. While 3 of the 4 GLCM parameters exhibit moderate to very good correlations with PFN and P_a, the parameter s-CLS in particular presents excellent correlations with both of the parameters. These results suggest that the s-CLS allows quantification of the increasing nuclear heterogeneity in cells undergoing apoptosis as a higher level of asymmetry in the fringe patterns presented in the diffraction image. We should note that reduced values of R^2 for the other 3 GLCM parameters may not necessarily mean that they cannot serve as good metrics of apoptosis since R^2 depends very sensitively on the noise in the data acquired by the three methods at different t_p. Future improvement in the p-DIFC instrumentation should significantly enhance the signal-to-noise ratios of the acquired diffraction images to enable the use of additional image parameters as quantitative and reliable markers of apoptosis.

Table 2. The values of R^2 on the correlation between the dependences of GLCM parameters and other parameters on t_p

	s-CLS	p-COR	p-CON	p-DIS
P_a by FCM	0.997	0.486	0.383	0.483
PFN	0.899	0.742	0.688	0.758

4. Discussion

Apoptosis is a cellular process of fundamental importance to many branches of life science and clinical research including gauging a cancer patient's response to treatment. Morphological changes such as cytoplasmic shrinkage, membrane blebbing, nuclear and cellular fragmentation are the defining features of apoptosis but they are difficult and labor intensive to quantify through microscopy. Instead, molecular assays have gained wide acceptance for detection of apoptosis and the Annexin V-FITC/PI assay through FCM in particular is the tool of choice for rapid measurement of apoptosis in single cells. In this report we presented the first results of apoptosis study in treated samples of HL-60 cells by three methods in which the new flow cytometric method of p-DIFC has been evaluated and validated against the established assays of fluorescence microscopy and FCM.

Fluorescence microscopy of treated cells has been conducted through quantitative analysis of the 2D morphology of the viable, early and late apoptotic cells to gain insights on their different characteristics. As can be seen in Table 1, strong and statistically significant differences exist between the viable cells and apoptotic cells for all 14 morphological parameters with $p<0.05$. Particularly, the values of area and perimeter both cell and nucleus decrease from the cases of viable cells to those of the apoptotic cells. These are accompanied by the gradual deviations of the suspension cells' shapes from the circular as they progress along the apoptosis process as demonstrated by the changes in the parameters of sphericity, elongation and aspect ratio. These results provide quantitative characterizations of the

#208709 - $15.00 USD Received 25 Mar 2014; revised 13 May 2014; accepted 8 Jun 2014; published 11 Jun 2014

defining features of nucleus shrinkage and fragmentation for apoptotic cells. It is worth mentioning that the degree of shrinkage in nuclei of apoptotic cells is markedly larger than that in cell as evidenced by the parameter of NCR in comparison to the viable cells.

A close examination of the diffraction image pairs of the viable and apoptotic cells shown in Fig. 1 reveals observable differences in their fringe patterns. To quantify the differences, a second order statistical method of GLCM has been applied to analyze the fringe patterns or image textures. The 4 GLCM parameters, CON, CLS, COR and DIS, that exhibit sensitive and consistent dependence on t_p as presented in Fig. 4 were selected as the initial morphological markers of apoptosis in single cells. It is interesting to note that the 4 GLCM parameters demonstrated opposite trends of variation with increasing t_p, which can be compared to the curves in Fig. 3(C) and the variations of 2D morphological parameters among the viable, early and late apoptotic cells as presented in Table 1. This fact points to the possibility of positive correlations between the group of GLCM parameters of CON and DIS and the group of morphological parameters of NCR and area, perimeter, ECD, sphericity, shape factor, diameter mean, diameter max, DIM related to cellular or its nuclear shape, and similarly between the group of CLS and COR and the group of elongation and aspect ratio for the cell. While the GLCM method provides a rapid approach for quantifying an image's textures, the GLCM parameters extracted from diffraction images exhibit convoluted correlations with the morphological parameters of 3D. As shown in Table 2, a strong correlation exists between P_a measured by the fluorescence microscopy and the FCM assay and the GLCM parameter of CLS obtained from the s-polarized diffraction images against t_p. To develop a better understanding of the parameter of CLS [34], we selected 4 s-polarized images from each of three cell samples of different t_p for visual examination. The diffraction images in Fig. 5 show a trend with the speckles appearing larger for cells with increasing t_p. The visual differences are consistent with the facts that apoptotic cells tend to have fragmented nuclei of reduced volumes which lead to larger speckles [25].

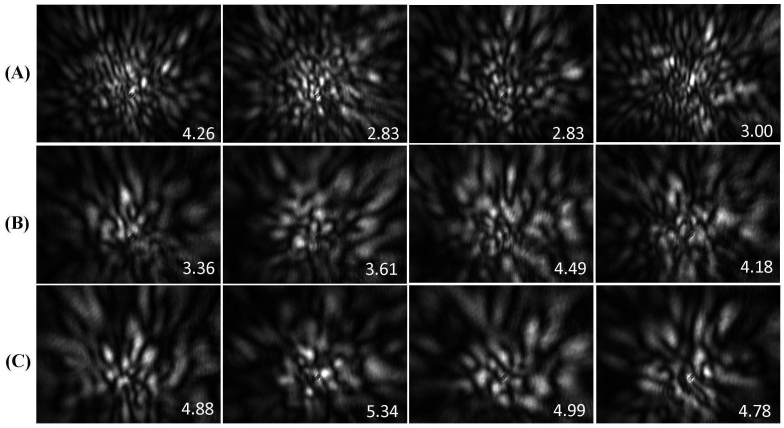

Fig. 5. Four s-polarized diffraction images from different cell samples with different values of t_p in hours: (A) 0; (B) 12; (C) 24. The number in each image is the value of s-CLS/10^5.

Despite the fact that the mean values of s-CLS increases with t_p as shown in Fig. 4(A), the actual values of s-CLS does not change monotonically with the variation of the speckle patterns as visually observed. Therefore, the parameter of s-CLS characterizes the texture in a quite complex fashion against the visual speckle patterns. A thorough understanding of the correlation between the GLCM parameters and the 3D morphology of the imaged cells requires powerful tools to accurately simulate the light scattering and consequent diffraction images with realistic cell models [21,25]. Study is currently under way in our group to develop the tools and investigate the correlations.

We note from Table 1 that statistically significant difference exist in the morphological parameters between the viable and apoptotic cells because of the deviation of apoptotic HL-

#208709 - $15.00 USD Received 25 Mar 2014; revised 13 May 2014; accepted 8 Jun 2014; published 11 Jun 2014

60 cells from the circular shapes and reduced sizes of the apoptotic cells. Taken together with the moderate to excellent correlations in terms of R^2 between the dependence of the 4 GLCM parameters and PFN on t_p, we conclude that the new method of p-DIFC has the capability to serve as a label-free means to analyze and measure apoptosis in single cells.

In summary, we have investigated and presented a new label-free method for the measurement of apoptosis in single HL-60 cells induced by H_2O_2 treatment with a p-DIFC technique that acquires cross-polarized diffraction image pairs rapidly from single cells without the need to stain them. The results of p-DIFC measurement of the control and treated cell samples were compared with the conventional fluorescence microscopy and FCM assays for evaluation and validation. We found that at least 4 parameters extracted from the diffraction image pairs based on a GLCM algorithm present strong correlations with the apoptosis rate determined by the FCM assay or the morphological changes of the cells undergoing apoptosis observed through microscopy.

Acknowledgments

The authors acknowledge grant supports from the Natural Science Foundation of China (#81171342, #81201148, #31000784) and the Tianjin Science & Technology Commission.

#208709 - $15.00 USD Received 25 Mar 2014; revised 13 May 2014; accepted 8 Jun 2014; published 11 Jun 2014